



# A Unit Cell with Tailorable Negative Thermal Expansion Based On a Bolted Additively Manufactured Auxetic Mechanical Metamaterial Structure: Development and Investigation

Erhard Buchmann<sup>1(✉)</sup>, Frank Hadwiger<sup>2,3</sup>, Christoph Petroll<sup>4</sup>,  
Christoph Zauner<sup>3</sup>, Alexander Horoschenkoff<sup>2</sup>, and Philipp Höfer<sup>1</sup>

<sup>1</sup> Institute of Lightweight Engineering, Universität der Bundeswehr München,  
Neubiberg, Germany

{erhard.buchmann, philipp.hoefler}@unibw.de

<sup>2</sup> Munich University of Applied Sciences, Munich, Germany  
alexander.horoschenkoff@hm.edu

<sup>3</sup> KRP Mechatec GmbH, Garching, Germany

hadwiger@krp-m.de, christoph.zauner@largespace.de

<sup>4</sup> Wehrwissenschaftliches Institut für Werk- und Betriebsstoffe, Erding, Germany  
christophpetroll@bundeswehr.org

**Abstract.** There is a growing interest in the application of mechanical metamaterials due to the recent advances in additive manufacturing technology. In particular, materials with adjustable thermal expansion have many fields of utilization in engineering. Materials with negative thermal expansion (NTE) can be used in combination with materials with positive thermal expansion for creating thermoelastically stable structures with an ultra low coefficient of thermal expansion (CTE). NTE-lattice structures generally require multi-material combinations to achieve the desired CTE. However, multi-material 3D printing is currently in development and not available for industrial-scale applications to date. In this paper, we present a unit cell based on an auxetic mechanical metamaterial structure that can be manufactured using single material additive manufacturing. For investigation, unit cells and a unit cell tessellation with certain CTEs were designed and manufactured using metallic materials. The mechanical and thermoelastic functionality of the designed unit cell could be demonstrated experimentally regarding the CTE and the stiffness. The presented approach for including cells with tuneable NTE and stiffness in additively manufactured structures has a high potential for realization in practice.

**Keywords:** Metamaterial · Smart materials · Negative thermal expansion · Additive manufacturing · Auxetic · Unit cell · Thermoelasticity

## 1 Introduction

Mechanical metamaterials have a rationally designed artificial micro structure that enables certain desired properties on macroscale [1]. Usually, the micro structure shows a unit cell that is composed periodically in order to create a macro scale structure. Due to the recent advances in additive manufacturing (AM) technologies, it is more and more possible to manufacture arbitrary complex geometries on several length scales for many materials which further advance this field of research [2, 3]. The properties of mechanical metamaterials encompass, but are not limited to, ultralight and ultrastiff structures [4], structures with a negative Poisson's ratio [5], and structures with a designed deformation pattern that facilitates building mechanisms [6]. This enables a wide range of application in engineering and science [3]. One class of metamaterials are thermoelastic metamaterials that have a designed coefficient of thermal expansion. On the one hand, they can serve as actuator [7, 8], on the other hand they can be used to design structures with a certain thermoelastic behavior [9, 10]. In particular, metamaterials with negative thermal expansion (NTE) can be used in combination with materials with positive thermal expansion for creating thermoelastically stable structures with ultra low coefficient of thermal expansion (CTE).

For the creation of NTE-metamaterials at least two components with different positive CTEs are required [11]. In order to achieve the desired overall thermal expansion, those constituents are arranged in special patterns, of which many have been proposed [12]. Many of these concepts have been tested using polymeric materials. But, for many applications, as an example for space applications, metallic materials are more suitable due to the higher temperature application range, better outgassing properties, and the superior stiffness.

Regarding the application of additive manufacturing, a major challenge is the joining of the two constituents. Multi-material additive manufacturing is currently in development and not available for industrial-scale applications to date. Interestingly, Ding et al. [13] fabricated a metallic metamaterial with NTE using a robotized laser powder-feed metal AM-system. As the authors were focusing on the manufacturing process, the functionality of the structure, especially the stiffness and the CTE were not examined. Parsons [14] investigated a NTE metamaterial structure of aluminum and titanium. He applied ultrasonic additive manufacturing to build a block structure with titanium and aluminum bands. This AM method has many limitation regarding the geometric complexity which was not further studied. The metamaterial structure was then cut out of this block. However, it is not addressed how the structure could be manufactured directly without an extra cutting process. Moreover, Parsons outlines different methods for manually joining (pins, bolts, interference fits, adhesives, soldering,

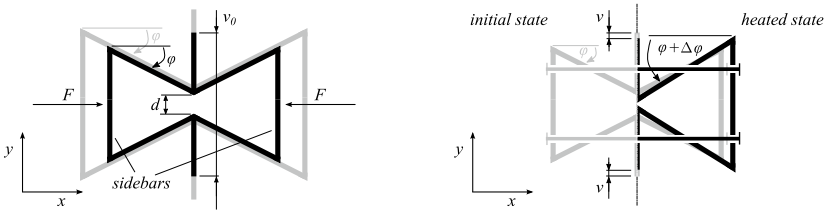
brazing or welding) applied in previous research work. Steeves et al. [15] investigated conventionally manufactured samples joined with interference fits, pins and bolts. These approaches of previous research work generally require the rather complex conventional manufacturing of two parts of different materials that are then joined. However, most of the studies to date focus on the investigation of underlying mechanisms of thermoelastic metamaterials. The design freedom when using additive manufacturing is generally not addressed. In particular, only limited studies show how to integrate thermoelastic metamaterials into components in practice. Moreover, the possibilities of AM for reducing post-processing as cutting and joining effort are not considered.

In this work, we present a unit cell with tailorable NTE based on an auxetic mechanical metamaterial structure that can be manufactured using single material AM and assembled straightforwardly using a customary screw. For investigation, unit cells and an unit cell tessellation with certain CTEs were designed and manufactured using aluminum. The functionality is then examined with tests regarding the stiffness and the CTE.

## 2 Design of the Unit Cells

### 2.1 Thermal Expansion Mechanism of the Unit Cell

The concept proposed herein is based on the auxetic planar cellular honeycomb structure, that was studied in [16–18] (see Fig. 1a).



(a) Auxetic honeycomb structure. Initial state (black) and heated state (grey). (b) Bolted auxetic honeycomb structure. Initial state (grey) and heated state (black, half model).

**Fig. 1.** Auxetic honeycomb structure without (a) and with (b) bolt showing the thermoelastic kinematics caused by thermal expansion

The re-entrant mechanism ensures the reduction of width  $v_0$  when stressed by the force  $F$  perpendicularly by a small increase of the angle  $\varphi$ . A uniform heating of the cell results in scaling of the structure without changing the angle  $\varphi$ . In this work, the thermal expansion of the unit cell in  $x$ -direction is hindered by using a bolt with a smaller CTE than the auxetic structure (see Fig. 1b). Due to the re-entrant mechanism, this results in a reduction of  $v_0$  by  $2v$  in the heated state.

So, a thermal expansion smaller than the CTE of the material of the auxetic structure  $y$ -direction, including NTEs can be realized. Simultaneously, the unit cell expands through the sidebars in  $y$ -direction. Consequently, a small gap  $d$  makes the thermal expansion mechanism efficient when aiming for NTEs. When subjected to temperatures under the installation temperature, the bolt must be preloaded to ensure the function of the re-entrant mechanism. This unit cell can be integrated into an arbitrary complex AM geometry for a local thermoelastic functionalization. By using a customary screw with nut as bolt, the structure can be assembled straightforwardly after 3D printing without extra manufacturing effort. The two main properties regarding the application, the stiffness and the CTE, substantially depend on the angle  $\varphi$ . The CTE was evaluated analytically using a quarter model which is outlined in the following.

### 2.2 Calculation of Thermoelastic Kinematics Caused by Thermal Expansion

For the calculation of the kinematics of thermal expansion an idealized truss model of the unit cell is considered. The truss consists of beams that are connected with ideal joints, whereby the joint stiffness is modeled with torsion springs (see Fig. 2a). In this course, the shear deformation and the bending deformation of the beams is neglected due to the low stiffness of the torsion springs in the experimental structures (see Sect. 2.3). The positions of the joints in the model refers to the experimental structures (see Fig. 4a). In Table 1 the main model parameters are listed.

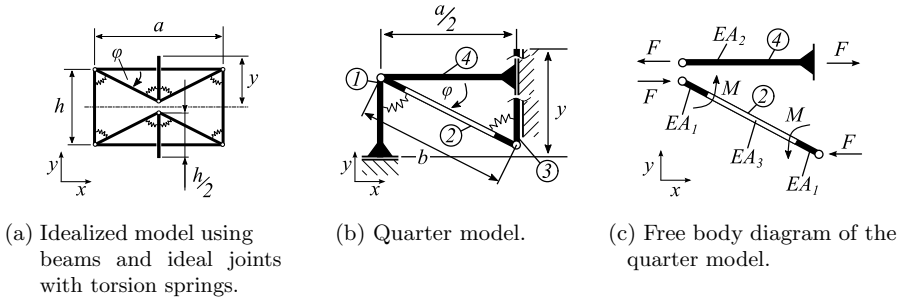


**Fig. 2.** Models used for the analytical calculation of the thermoelastic kinematics caused by thermal expansion. Beam 2 has two axial stiffnesses,  $EA_1$  (black sectors) and  $EA_3$  (white sector). Beam 4 has the axial stiffness  $EA_2$

Due to the symmetry, the study of a quarter model is adequate (see Fig. 2b). For the beams two coefficients of thermal expansion  $\alpha$  are regarded,  $\alpha_1$  (beams 1, 2, 3) and  $\alpha_2$  (beam 4), with  $\alpha_1 > \alpha_2$ . For the calculation all beams are subjected to the same temperature load  $\Delta T$  and are subjected to the reaction forces in the joints. Consequently, the total expansion of a beam of the length  $l$  is the

sum of two parts. On the one hand the thermal expansion  $\Delta l_{th}$ , on the other hand the mechanical expansion through the reaction forces  $\Delta l_m$ . The thermal expansion  $\Delta l_{th}$  is considered as  $\Delta l_{th} = l \cdot \alpha \cdot \Delta T$ . For the mechanical expansion  $\Delta l_m$  through the force  $F$  the linear formula  $\Delta l_m = l \cdot \frac{F}{EA}$  using the axial stiffness  $EA$  is applied. Two axial stiffnesses for beam 2 are considered (see Fig. 2).  $EA_1$  is the axial stiffness of the hinges whereas  $EA_3$  is the axial stiffness of the solid part of beam 2. The axial stiffness of the solid part is far higher than the axial stiffness of the hinges at the experimental structures in this work (see Sect. 2.3). Therefore, the solid part is seen as rigid here.

**Table 1.** Main model parameters for the calculation of the thermoelastic kinematics caused by thermal expansion

Symbol	Description
$\Delta l_{th}$	Thermal expansion
$\Delta l_m$	Mechanical expansion
$\alpha_1$	Coefficient of thermal expansion of beams 1, 2, 3
$\alpha_2$	Coefficient of thermal expansion of beam 4
$EA_1$	Axial stiffness of the hinges adjacent to beam 2
$EA_2$	Axial stiffness of beam 4
$EA_3$	Axial stiffness of beam 2
$C$	Joint stiffness
$a$	Unit cell dimension in $x$ -direction
$b$	Length of re-entrant mechanism leg
$h$	Unit cell dimension in $y$ -direction
$\varphi$	Angle of re-entrant mechanism

In order to calculate the reaction forces a free body diagram is investigated (see Fig. 2c). In this course, the change of the angle  $\varphi$  of the re-entrant mechanism when heated is described with  $\Delta\varphi$ . Each torsion spring with stiffness  $C$  at the joints then introduce the moment  $M = C \cdot \Delta\varphi$  on beam 2. The equilibrium of moments for beam 2 of length  $b$  gives

$$F = \frac{2 \cdot C \cdot \Delta\varphi}{b \cdot \sin(\varphi + \Delta\varphi)}. \quad (1)$$

For the total expansion in  $y$ -direction, the geometric compatibility of beam 2 and 4 must be met:

$$\frac{a}{2} + \Delta l_{th_4} + \Delta l_{m_4} = (b + \Delta l_{th_2} + \Delta l_{m_2}) \cdot \cos(\varphi + \Delta\varphi) \quad (2)$$

When using the formulas for  $\Delta l_{th}$ ,  $\Delta l_m$  together with Eqs. (1) and (2), the angular change  $\Delta\varphi$  and the reaction force  $F$  can be calculated.

In order to determine the CTE of the unit cell the section  $y$  in undeformed state ( $y_0$ ) and in heated state ( $y_{th}$ ) is calculated. The sections  $y_0$  and  $y_{th}$  can be described as follows.

$$y_0 = h - \frac{a}{2} \cdot \tan\left(\arccos\left(\frac{a}{2 \cdot b}\right)\right) \quad (3)$$

$$y_{th} = h + \alpha_1 \cdot h \cdot \Delta T - \tan(\varphi + \Delta\varphi) \left[ \left( \frac{a}{2} + \alpha_2 \cdot \frac{a}{2} \cdot \Delta T + \frac{F}{EA_1} \cdot \frac{a}{2} \right) \right] \quad (4)$$

This gives for the CTE in  $y$ -direction of the whole unit cell

$$CTE_y(a, b, h, \alpha_1, \alpha_2, \varphi, \Delta T, EA_1, EA_2, C) = \frac{y_{th} - y_0}{y_0 \cdot \Delta T} \quad (5)$$

The CTE in  $x$ -direction is the same as for beam 4.

$$CTE_x(a, b, h, \alpha_1, \alpha_2, \varphi, \Delta T, EA_1, EA_2, C) = \frac{\Delta l_{m_4} + \Delta l_{th_4}}{\frac{a}{2} \cdot \Delta T} = \frac{F}{EA_2 \cdot \Delta T} + \alpha_2 \quad (6)$$

Notably, beams 2 and 4 are stretched or compressed respectively during heating depending on the ratio of the axial stiffnesses and the joint stiffness. In the following, the governing equations shall be used to design the experimental unit cells and the unit cell tessellation.

### 2.3 Design of Experimental Unit Cells

Equations (5) and (6) show that the CTEs can be influenced by many material and geometric parameters. For the selection of materials see Sect. 3.1. In order to provide adequate reference surfaces for the capacitive displacement sensors, a depth of 15 mm was chosen (see Table 2 and Fig. 4b).

To guarantee the system kinematics, hinges were used as joints. Hinges can be manufactured directly and need no further mounting procedure. As thickness of the hinges 0.5 mm was used. Preliminary experiments showed that these hinges can be manufactured robustly and provide enough flexibility. Hence, the beams were designed to 3 mm, to have a significant higher cross section of the beams compared to the hinge. The hinge stiffness  $C$  was determined experimentally (3000 Nmm rad<sup>-1</sup>). The expansion mechanism requires a hole in beam 2 for the bolt (see Fig. 4a). For the calculation, the influence of the hole on the axial stiffness on beam 2 is neglected. Moreover, as to prevent the hole passing through the hinges, the angle must be reasonably large.

This work focuses on studying the influence of the angle  $\varphi$ . In order to make the unit cells comparable, a constant width  $a$  of 60 mm and a constant gap  $d$  of 1 mm was utilized. Consequently,  $b$  and  $h$  are depended parameters that can be calculated as follows.

$$b = \frac{a}{2} \cdot \cos(\varphi) \quad (7)$$

$$h = a \cdot \sin(\varphi) + 1 \text{ mm} \quad (8)$$

**Table 2.** Main geometric dimensions for the three investigated unit cells (UC+3, UC-16, UC-71)

Parameter type	Value	Unit	UC+3	UC-16	UC-71
Design target	$CTE_y$	$10^{-6} \text{ K}^{-1}$	2.7	-15.8	-70.6
Variable	$\varphi$	$^\circ$	37.6	28.3	18.5
	$a$	mm	60		
	$d$	mm	1		
Constant	$C$	$\text{Nmm rad}^{-1}$	3000		
For all unit cells	Depth of models	mm	15		
	Thickness of beams	mm	3		
	Thickness of hinges	mm	0.5		
Dependent	$b$	mm	37.9	34.1	31.6
	$h$	mm	47.2	33.3	21.1
	$CTE_x$	$10^{-6} \text{ K}^{-1}$	9.7	9.7	9.7

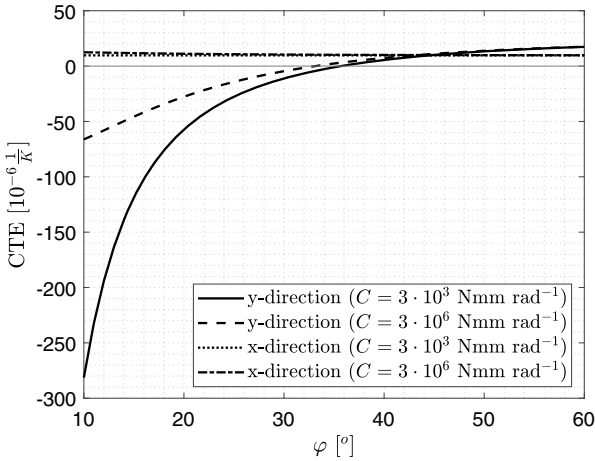


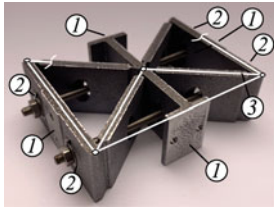
**Fig. 3.** Influence of the angle  $\varphi$  on the CTEs using the values of Tables 2 and 3. While  $CTE_x$  stays almost constant at approx.  $9.7 \cdot 10^{-6} \text{ K}^{-1}$  for all  $\varphi$ , the  $CTE_y$  asymptotically approximates the CTE of the auxetic base material with rising  $\varphi$ . For decreasing  $\varphi$  the  $CTE_y$  gets more sensitive to changes of  $\varphi$ . Negative CTEs in  $y$ -direction can be realized with angles smaller than approx.  $36^\circ$ . The influence of the torsion stiffness  $C$  is very small here. Only when using a value far higher ( $C = 3 \cdot 10^6 \text{ Nmm rad}^{-1}$ ) instead of  $C = 3 \cdot 10^3 \text{ Nmm rad}^{-1}$  a notable deviation can be seen

The target coefficient of thermal expansion  $CTE_y$  can now be designed using the angle  $\varphi$  (see Fig. 3).

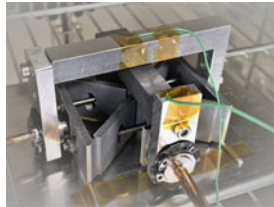
$CTE_x$  stays almost constant at approximately  $9.7 \cdot 10^{-6} \text{ K}^{-1}$  for all  $\varphi$ . The  $CTE_y$  asymptotically approximates the CTE of the auxetic base material with rising  $\varphi$ . Notably, all the designed  $CTE_y$  are smaller than those of the auxetic base material. For decreasing  $\varphi$ , the  $CTE_y$  gets more sensitive to changes of  $\varphi$ . Negative  $CTEs$  in  $y$ -direction can be realized with angles smaller than approximately  $36^\circ$ .

The influence of the torsion stiffness  $C$  is very small for the structure investigated here. Only when using a value far higher a notable deviation can be seen (see Fig. 3). In this case the thermal expansions of the beams  $\Delta l_{th}$  stay the same while the mechanical expansions get higher due to the higher reaction forces (see Eq. 1). This results in a more positive CTE in  $x$  and  $y$ -direction. Notably, the mechanism is stressfree for any thermal state if  $C = 0$  is applied (see Eq. 1).

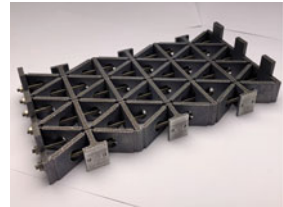
For the experimental test, unit cells (UC) with  $CTE_y$  of  $+2.7 \cdot 10^{-6} \text{ K}^{-1}$  (UC+3),  $-15.8 \cdot 10^{-6} \text{ K}^{-1}$  (UC-16, see Fig. 4a) and  $-70.6 \cdot 10^{-6} \text{ K}^{-1}$  (UC-71) were designed (see Table 2). As the mechanical expansion is very small, the  $CTE_x$  of  $9.7 \cdot 10^{-6} \text{ K}^{-1}$  differs insignificantly from the one of titanium. Moreover, a 3x3 tessellation structure of the UC-16 unit cells (UCM-16) was investigated (see Fig. 4c).



(a) Unit cell UC+3 with grinded surfaces for the measurement rig with displacement sensors (1) and the titanium screws (2). The calculation model (3) refers to the center lines.



(b) Unit cell UC+3 with measurement rig, displacement and temperature sensors.



(c) Matrix unit cell structure (UCM-16).

**Fig. 4.** Investigated unit-cell UC+3 without (a) and with measurement equipment (b). Unit cell tessellation structure (UCM-16) (c). In (a) the deviation of the position of the joints in the calculation model and the position of the hinges of the printed structure can be seen



### 3 Materials, Manufacturing and Experimental Procedure

#### 3.1 Materials

An aluminum alloy was used for the AM structure as it is a common material for structural applications. Moreover, additive manufacturing facilities for aluminum alloys are wide spread in industry. For the bolt a M3 titanium threaded rod with nuts and washers was used. The combination of titanium and aluminum forms a notable CTE gap what allows the effective creation of the thermal expansion properties of the metamaterial. For the determination of the coefficients of thermal expansion of both metals a thermomechanical analysis (TMA) was applied.

**Table 3.** Material data for analysis. Mean CTEs for temperatures between 20 °C and 135 °C were measured using TMA

Material	CTE (TMA)	Young's modulus [19]
Aluminum (AlSi10Mg)	$21.1 \cdot 10^{-6} \text{K}^{-1}$	69 GPa
Titanium (Grade 2)	$9.7 \cdot 10^{-6} \text{K}^{-1}$	110 GPa

#### 3.2 Manufacturing and Experimental Procedure

For the unit cells and the unit cell tessellation selective laser sintering (SLS) parts were manufactured. In order to avoid support structure in the AM process, the holes for the titanium bolt in the auxetic base structure were designed elliptic. The M3 titanium threaded rods were mounted to the manufactured structure with a torque of <1 Nm using a high-precision torque wrench. This preload was enough to avoid a settling effect during heat up and to limit the elastic deformation through the preload to a minimum. The auxetic part has functional surfaces for placing the measurement rig with displacement sensors and the titanium threaded rod with washer which is depicted in Fig. 4a. All functional surfaces are protruded and could be grinded after the additive manufacturing.

For the examination of the mechanical and thermoelastic functionality two types of experiments were conducted. (i) The stiffness in  $y$ -direction was evaluated using a common tensile testing machine. With the actual design, the unit cell can only be loaded by traction. (ii) The thermoelastic characterization test was performed in a heating chamber with circulating air. The forced convection ensures a nearly homogeneous heat up of all areas of the specimen. Two cycles from room temperature to 135 °C were performed. The temperature was measured redundant at the surface using two thermocouples. The deformations of the unit cell in  $x$ -direction and  $y$ -direction were measured contact-free with capacitive displacement sensors. The displacement sensors have a measurement accuracy of  $\pm 0.03\%$ . Measurement rigs were manufactured during the same printing

job than the samples. The rig is mounted on one side to the mounting reference surface of the specimen and on the other side the displacement sensor is applied. The temperature dependent CTE of the rig is well known by a TMA measurement and can be compensated afterwards. Hence, the expansion of the specimens can be measured suitable. The instantaneous CTE was evaluated for each measurement according to ASTM-E228-17 [20].

## 4 Experimental Results and Discussion

### 4.1 Test of the Biaxial Thermal Expansion Behavior

The measured mean CTEs in  $x$  and  $y$ -direction were compared to the calculated CTEs which is depicted in Fig. 5. Generally, there is a good concordance of the calculated values of  $CTE_y$  to the measured ones regarding the unit cells. Consequently, the concept is appropriate for designing unit cells with positive CTEs smaller than the auxetic base material to unit cells with a high NTE. The concurrence for the unit cells UC+3 and UC-16 with a deviation of  $0.6 \mu\text{m}$  and  $1.7 \mu\text{m}$  respectively is better compared to the UC-71 with a deviation of  $9.2 \mu\text{m}$ . Hence, there is a higher deviation between the measured  $CTE_y$  compared to the calculated values at lower values of the CTE. In this work, lower values of the CTE are reached with lower angles  $\varphi$ . This is in accordance with the angular sensitivity of the unit cells. The unit cell is more sensitive for changes in  $\varphi$  for lower values of  $\varphi$ , which can be seen in Fig. 3. Consequently, the discrepancies in the angle  $\varphi$  between the calculation model and the experimental structure result in higher deviations of the measured CTEs compared to the calculated ones at lower angles  $\varphi$ . Regarding the inclination of  $CTE_y$  with respect to  $\varphi$ , the change in sensitivity is nonlinear and much higher at angles lower than approximately  $20^\circ$  (see Fig. 3). Therefore, the deviations of  $CTE_y$  are comparable at UC+3 and UC-16, and much higher at UC-71.

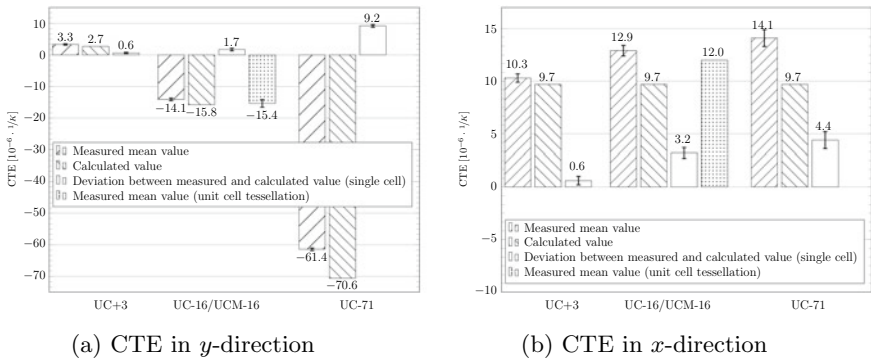


**Fig. 5.** CTEs in  $x$  and  $y$ -direction of the investigated unit cells (UC+3, UC-16, UC-71) and the unit cell matrix (UCM-16)

The deviation of  $CTE_x$  rises with lower angles or lower CTEs respectively, too. While the deviation of  $CTE_x$  at UC-71 is 4.4  $\mu\text{m}$ , it is lower for UC-16 (3.2  $\mu\text{m}$ ) and for UC+3 (0.6  $\mu\text{m}$ ). Regarding the unit cell tessellation, the deviation of  $CTE_y$  is higher compared to the unit cell, while the deviation of  $CTE_x$  is lower.

It is assumed that there are two main reasons for the deviations of the measured values. First, there are inaccuracies related to the joining of the titanium threaded rods. The holes in the auxetic structure for the bolts provide a very loose fit to the titanium threaded rods. Therefore, the two rods could be assembled non-parallelly. Secondly, there are geometric deviations of the calculation model compared to the printed structure (see Fig. 4a). The titanium screw is larger than in the calculation model caused by the thickness and the protrusion on the aluminum beams. Therefore, the expansion of the unit cell in  $x$ -direction is higher, which is in accordance with the measured values of  $CTE_x$  (see Fig. 5b). Moreover, this lowers the re-entrant effect of the mechanism. This could contribute to the lower measured NTE values of  $CTE_y$  of UC-71 and UC-16. Also, this matches with the lower deviation of  $CTE_x$  and  $CTE_y$  of the unit cell tessellation. There, the thickness of the aluminum truss and the protrusion contribute only two times for three unit cells. Therefore, the overlength of the titanium threaded rod with respect to the calculation model is shorter per unit cell compared to the single cell model.

Another point is the deviation of the joint position between the calculation model and the printed structure. At the printed structure, the length  $h$  is shorter which lowers the CTE in  $y$ -direction. This is in accordance with the lower measured CTE compared to the calculated one of UC+3. Moreover, the truss  $b$  is shorter, which results in a shorter lever arm of the re-entrant mechanism and therefore a reduction of the NTE-effect in  $y$ -direction. This is in coincidence with UC-16 and UC-71.

During the measurement a strong dependence of the CTEs of the temperature was observed, which is depicted exemplary for UC-16 in Fig. 6a. Therefore, a temperature-dependent calculation of the CTEs of the unit cell UC-16 was applied using the temperature-dependent CTEs of aluminum and titanium measured in the TMA. Both measured CTEs of the unit cell increase with rising temperature rather linearly which is in good accordance with the calculated CTEs. In concordance with the mean CTEs the deviation of  $CTE_x$  is bigger than  $CTE_y$ . In future, the temperature-dependent behavior should be further investigated.

It could be shown that with this unit cell wide ranges of CTEs and NTE can be realized. Hence, the unit cell can serve as a thermal actuator or as designed compensation actuator for a structures with a longer characteristic length than the unit cell with positive CTE.

In the experiments the unit cells were only investigated over the installation temperature, as the mechanism does not work at lower temperatures with the small preload. This can be overcome by assembling the mechanism under

the operating temperatures, by using higher preloads or by locking the axial movement of the titanium rods in both directions.

As can be seen in Eq. (5) there are many possibilities to increase the CTE efficiency of the unit cell. Regarding Eq. (4), one possibility for improving the NTE-effect would be to lower  $\alpha_2$ . On the one hand, this could be done using a carbon fiber as rod instead of the titanium threaded rod. On the other hand, a rod made of shape memory alloy could be utilized to further increase the NTE-effect. As the reaction forces are rather low, rods with far lower axial stiffness, e.g. wires, are suitable as well, when only stiffness for tensile loads on the unit cell is required. This would further broaden the possibility for integrating this unit cell into components. After the manufacturing of a component with several unit cells in arbitrary positions the wire could be run in afterwards through all cells serving as rod.

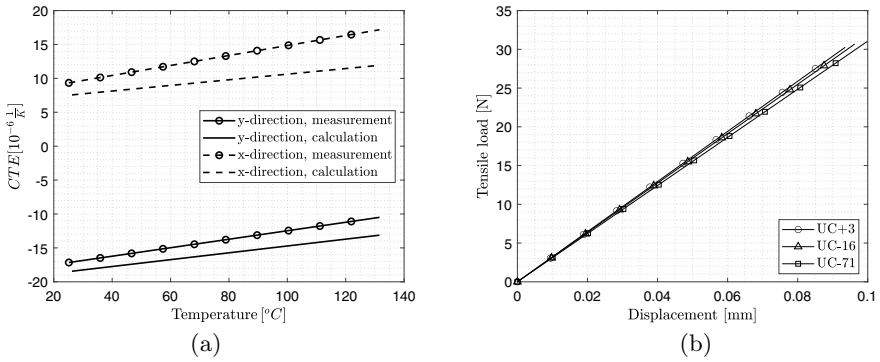


**Fig. 6.** Temperature-dependent CTEs of the UC-16 unit cell (a) and stiffness in  $y$ -direction of UC+3, UC-16, UC-71 (b)

### 4.2 Test of Stiffness in the Direction of Thermal Expansion

Besides the kinematics of thermal expansion, the mechanical properties have to be considered when applying the unit cells into components. In general, the CTEs and the stiffness of the unit cell depend on each other (see Sect. 2.2). Notably, cells with lower NTE have smaller angles  $\varphi$ . This results in higher reaction forces under thermal loads, which can be deduced from Eq. (2). But, because of the low torsion stiffness, the reaction forces are very small (see Eq. (1)). Consequently, the mechanical elongation of the trusses under thermal loads can be neglected here.

Regarding the mechanical properties, the stiffness of the unit cells in the direction of thermal expansion was tested experimentally. The tensile test of the three unit cells showed a similar stiffness value and a similar linear behavior of the tensile load with respect to the deformation (see Fig. 6b). In this course, the

stiffness slightly decreases with higher angles. This behavior can be explained with an increasing shear deformation of the hinges at lower angles.

## 5 Conclusion

In this paper we designed and investigated a unit cell with tailorable CTE based on a bolted additively manufactured auxetic mechanical metamaterial structure. First, the thermoelastic behaviour was studied analytically to predict the thermal expansion for the designed unit cells. Then the thermoelastic functionality was assessed experimentally for three different unit cells and an unit tessellation. Additionally, the stiffnesses of the respective unit cells were evaluated by a mechanical loading test. A good concordance between the calculated and measured CTEs was found in a wide range of CTEs, including a low thermal expansion ( $3.3 \cdot 10^{-6} \text{ K}^{-1}$ ) and a highly negative CTE of  $-61.4 \cdot 10^{-6} \text{ K}^{-1}$ . Hence, the presented unit cell concept can be applied as thermal actuator or compensation unit for structures with positive CTE for reaching ultra low thermal expansion of a component. Importantly, it could be shown that the presented manufacturing approach using single material additive manufacturing and then fitting a customary screw has a high potential to be applied in practice.

**Acknowledgments.** This work was supported by the dtec.bw—Digitalization and Technology Research Center of the Bundeswehr through the Project SeRANIS—Seamless Radio Access Networks in the Internet of Space under Grant 150009910. We also greatly acknowledge the support of KRP Mechatec GmbH and Wehrwissenschaftliches Institut für Werk- und Betriebsstoffe.

## References

1. A.A. Zadpoor, *Materials Horizons* **3**(5), 371 (2016)
2. M. Askari, D.A. Hutchins, P.J. Thomas, L. Astolfi, R.L. Watson, M. Abdi, M. Ricci, S. Laureti, L. Nie, S. Freear, et al., *Additive Manufacturing* p. 101562 (2020)
3. J.U. Surjadi, L. Gao, H. Du, X. Li, X. Xiong, N.X. Fang, Y. Lu, *Advanced Engineering Materials* **21**(3), 1800864 (2019)
4. X. Zheng, H. Lee, T.H. Weisgraber, M. Shusteff, J. DeOtte, E.B. Duoss, J.D. Kuntz, M.M. Biener, Q. Ge, J.A. Jackson, et al., *Science* **344**(6190), 1373 (2014)
5. A. Joseph, V. Mahesh, D. Harursampath, *Advances in Manufacturing* **9**(3), 342 (2021)
6. A. Ion, J. Frohnhofen, L. Wall, R. Kovacs, M. Alistar, J. Lindsay, P. Lopes, H.T. Chen, P. Baudisch, in *Proceedings of the 29th annual symposium on user interface software and technology* (2016), pp. 529–539
7. O. Sigmund, S. Torquato, *Applied Physics Letters* **69**(21), 3203 (1996)
8. M.M. Toropova, C.A. Steeves, in *Smart Materials, Adaptive Structures and Intelligent Systems*, vol. 57298 (American Society of Mechanical Engineers, 2015), vol. 57298, p. V001T01A002
9. N. Yamamoto, E. Gdoutos, R. Toda, V. White, H. Manohara, C. Daraio, *Advanced Materials* **26**(19), 3076 (2014)
10. M.M. Toropova, C.A. Steeves, *Acta Astronautica* **113**, 132 (2015)

11. A.L. Kalamkarov, A.G. Kolpakov, *Analysis, design and optimization of composite structures*, vol. 1 (Wiley New York, 1997)
12. H. Xu, A. Farag, D. Pasini, *Journal of the Mechanics and Physics of Solids* **117**, 54 (2018)
13. Y. Ding, M. Akbari, X.L. Gao, L. Ai, R. Kovacevic, in *Manufacturing techniques for materials: engineering and engineered* (CRC Press, 2018), pp. 51–65
14. E.M. Parsons, *Composite Structures* **223**, 110656 (2019)
15. C.A. Steeves, S.L.d.S. e Lucato, M. He, E. Antinucci, J.W. Hutchinson, A.G. Evans, *Journal of the Mechanics and Physics of Solids* **55**(9), 1803 (2007)
16. L.J. Gibson, M.F. Ashby, G. Schajer, C. Robertson, *Proceedings of the Royal Society of London. A. Mathematical and Physical Sciences* **382**(1782), 25 (1982)
17. R. Almgren, *J. Elast* **15**, 427 (1985)
18. T.L. Warren, *Journal of applied physics* **67**(12), 7591 (1990)
19. D.A. de Rooij. Spacematdb - space material database. <https://www.spacematdb.com/spacemat/>
20. ASTM International, Standard test method for linear thermal expansion of solid materials with a push-rod dilatometer. Standard ASTM E228-17, West Conshohocken, PA (2017)